ADVANCED FUNCTIONAL MATERIALS
www.afm-journal.de

www.MaterialsViews.com

Synthesis of Dumbbell-Like Gold–Metal Sulfide Core–Shell Nanorods with Largely Enhanced Transverse Plasmon Resonance in Visible Region and Efficiently Improved Photocatalytic Activity

Liang Ma, Shan Liang, Xiao-Li Liu, Da-Jie Yang, Li Zhou, and Qu-Quan Wang**

The metallic nanostructures with unique properties of tunable plasmon resonance and large field enhancement have been cooperated with semiconductor to construct hetero-nanostructures for various applications. Herein, a general and facile approach to synthesize uniform dumbbell-like gold–sulfide core–shell hetero-nanostructures is reported. The transformation from Au nanorods (NRs) to dumbbell-like Au NRs and coating of metal sulfide shells (including Bi_2S_3, CdS, Cu_xS, and ZnS) are achieved in a one-pot reaction. Due to the reshaping of Au core and the deposition of sulfide shell, the plasmon resonances of Au NRs are highly enhanced, especially the about 2 times enhancement for the visible transverse plasmon resonance compared with the initial Au NRs. Owing to the highly enhanced visible light absorption and strong local electric field, we find the photocatalytic activity of dumbbell-like Au–Bi_2S_3 NRs is largely enhanced compared with pure Bi_2S_3 and normal Au–Bi_2S_3 NRs by testing the photodegradation rate of Rhodamine B (RhB). Moreover, the second-layer sulfide can be coated and the double-shell Au–Bi_2S_3–CdS hetero-nanostructures show further improved photodegradation rate, especially about 2 times than that of Degussa P25 TiO_2 (P25) ascribing to the optimum band arrangement and then the prolonged lifetime of photo-generated carriers.

1. Introduction

The new design of functional materials with excellent photoelectrical and photoelectrochemical properties is critically important for solving the problems of energy crisis and environment pollution. Different semiconductor materials (such as TiO_2, CdS, and ZnO) have received widespread attention due to their special physical and chemical properties favored for dye-sensitized solar cells (DSSCs), photodegradation of organic pollutants, and hydrogen generation.[1–8] However, the high recombination ratio of photo-induced electron–hole pairs and the limited utilization of broad band light for a single-component semiconductor restrict its performance in device application under solar light irradiation.[4,9–11] The synthesis and investigation of hetero-nanostructures with different constituents and optical response have experienced a rapid development in recent years. Because of integrating characteristic properties of different constituents and generating new properties caused by the inter-material interaction, the hetero-nanostructures have excellent manifestation in the process of photon–electron conversion.[12–17]

Metal nanocrystals with unique surface plasmon resonances (SPRs) are regarded as a fascinating component in the hetero-nanostructures. To combine different metal nanoparticles (Au, Ag, and Pt) with semiconductor also had been a hot topic in recent decades. The contact of metal and semiconductor can produce an active interface, and the interfacial charge separation and resonant energy transfer are complex, while some positive factors could improve the efficiency of photon–electron conversion.[18,19] The plasmonic resonances lead to the great absorption cross-section and make metallic nanocrystals an ideal light-harvesting medium.[20] Some recent research progresses of hot electron injection into semiconductors provide an alternative utilization of light as well.[21–23] The large scattering ability of plasmon could prolong the light pathway and then improve the light absorption of adjacent semiconductor.[24–26] Moreover, the plasmon induced local field enhancement could enhance the light-semiconductor interaction and increase the quantity of photo-generated carriers in the semiconductor adjacent to the metal,[27,28] especially for the part near the surface, the electron–hole recombination could be suppressed due to

L. Ma, X.-L. Liu, D.-J. Yang, Dr. L. Zhou, Prof. Q.-Q. Wang
Department of Physics
Key Laboratory of Artificial Micro- and Nano-structures of the Ministry of Education
Wuhan University
Wuhan 430072, P.R. China
E-mail: zhouli@whu.edu.cn; qqwang@whu.edu.cn
Dr. S. Liang
Department of Physics
Hunan Normal University
Changsha 410081, P.R. China
Prof. Q.-Q. Wang
Institute for Advanced Study
Wuhan University
Wuhan 430072, P.R. China

DOI: 10.1002/adfm.201403398

the short diffusion length to the surface for redox reactions. Otherwise, the metallic nanocrystals could also act as an electron acceptor and improve the lifetime of photo-generated electrons.[29–31]

The arrangement of hetero-nanostructures is important for the final performance. Janus-like and core–shell are two typical structural motifs.[32,33] The core–shell structures have special advantages of maximizing the active interface and protecting the core metal from corrosion and reshaping, which is very important because the plasmon properties are greatly determined by the size and shape of metallic nanocrystals.[34–38] Compared with spherical nanoparticles, Au nanorods (NRs) have anisotropic morphology and then exhibit two plasmon resonances termed as transverse SPRs (T-SPRs) and longitudinal SPRs (L-SPRs).[39] Au NRs have been coupled with various metal oxide materials (SiO_2, TiO_2, Cu_2O, Fe_xO_y, CeO_2, etc.) and metal sulfide materials (CdS, ZnS, Ag_2S, Cu_xS, etc.) to form hetero-nanostructures.[40–48] An outstanding advantage of Au NRs is that the L-SPRs could be easily tuned in near infrared (NIR) region by adjusting the aspect ratio. Most interesting, the T-SPR band located in the visible region is stable and excellently matches the peak wavelength of solar spectrum. That implies Au NRs have the potential to be incorporated into the solar applications. However, in extinction spectra, the intensity of T-SPRs is only 20%–40% of L-SPRs, which indicates the harvesting of visible light energy is limited for Au NRs.

In this work, we report a facile and common method to synthesize the dumbbell-like Au–sulfide core–shell NRs. Accompanying with the coating of metal sulfides (including CdS, Bi_2S_3, ZnS, and Cu_xS), the morphology of Au NRs synchronously transforms to the dumbbell-like shape. Although the dumbbell-like Au have been produced through the controlled overgrowth of Au NRs stabilized by cetyltrimethylammonium bromide (CTAB),[49–54] the further growth of metal sulfide onto them with complete single or multi shell as well as maintaining the shape is not easy. Normally, the growth of semiconductor sulfide shells onto Au nanocrystals is very difficult due to the large lattice mismatch between the two materials.[55] Binding metal ion–molecule complex as precursor onto Au, applying Ag_2S shells as intermediate layer and cation exchange method have been successfully demonstrated to prepare the metal–semiconductor core–shell hybrids.[45,56] Ascorbic acid (AA) has been exhibited to cooperate with CTAB for growing the uniform and dense semiconductor oxide shell onto various metal nanoparticles.[57] Here, Au NR reshaping to dumbbell-shape and the sulfide shell growth are accomplished in one-pot reaction. The cooperative effect of CTAB, AA, and S source (thioacetamide, TAA) is studied. Compared with the initial Au NRs, the dumbbell-like Au NRs exhibit greatly enhanced T-SPR in visible region, which is a particular advantage to improve the visible light harvesting (the main portion in the solar spectrum). We also demonstrate the outstanding photocatalytic activity of these dumbbell-like Au–sulfide core–shell NRs with monolayered and double-layered sulfide shells. Two metal sulfides of CdS and Bi_2S_3 are shown in the photocatalytic experiments. CdS is expected as an ideal semiconductor material for solar devices with the bulk bandgap of ≈2.4 eV (≈510 nm), which is perfectly matched with the solar light as well as with the T-SPR of Au NRs here. Bi_2S_3 is a layer-structured semiconductor with narrow bulk bandgap (≈1.3 eV) and high absorption coefficient, thus exhibits great potential in photocatalysis, photodetector, and photovoltaics recently. Here, several advantages of Au–sulfide core–shell NRs: 1) dumbbell-like Au NRs with strongly enhanced T-SPRs and tunable L-SPRs; 2) stronger local electric field induced by the dumbbell-like shape as compared to initial Au NRs; 3) integrating dumbbell-like Au NRs with excellent semiconductor materials of CdS and Bi_2S_3; 4) good spectral overlap between CdS bandgap and T-SPR wavelength as well as Bi_2S_3 bandgap and L-SPR wavelength, make the materials as an ideal candidate for the optoelectronic applications.

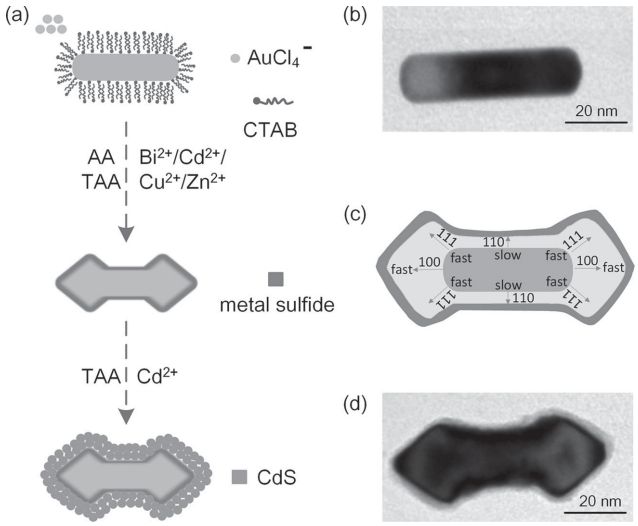

Figure 1. a) Schematic illustrating the preparation of dumbbell-like Au–metal sulfide core–shell nanostructures. A single Au NR b), possible growth mechanism c), and a single dumbbell-like Au–Bi_2S_3 NR d) are displayed.

2. Results and Discussion

2.1. Synthesis and Characterization

The reshaping of Au NRs and the coating of metal sulfides could be accomplished in one-pot reaction and the detail approach for synthesizing dumbbell-like gold–metal sulfide NRs is shown progressively in **Figure 1**a. The dumbbell-like shape was produced through the reduction of residual chloroauric acid by AA in the uncentrifuged Au NRs solution and the overgrowth of Au on the initial Au NRs. The initial Au NRs were synthesized by the conventional seed-mediated method using CTAB as the surfactant. Previous literatures have revealed that the surfactants of CTAB are expected to bind much more strongly to the {110} surface (dominate the side facets of Au NRs) than to the {111} or {100} facets (enclose the ends of Au NRs).[58,59] As shown in Figure 1b–d, the dumbbell-like NRs with enlarged diameter and length could be produced through the controlled overgrowth (higher overgrowth rate along {111} directions than that along {110} directions) of Au on the CTAB-stabilized Au NRs, which were analogous reported before.[58,60,61] It should be noticed that the reaction is performed in the presence of S source (TAA) and metal ion source (metal acetate). Previous

report shows the crystalline growth directions can be further regulated by adding foreign ions (such as Ag^+ ions) or by using different reduction methods.[62] Sulfide has also been reported to induce the selective growth of gold by reduction or quenching of Au precursor as well as the adsorption of sulfide onto the Au NRs surface.[63] Hence, we think that the presence of CTAB surfactant and TAA (or generated sulfide) played a co-promoted role in the formation of the dumbbell-like Au NRs. TAA, AA, and CTAB are also critically important for the semiconductor growth besides the reshaping of Au NRs (Figures S1 and S2, Supporting Information). TAA was regard as the S source and could combine with metal ions to form metal sulfide shells deposited onto Au NRs. For depositing complete and dense semiconductor shells on metallic nanoparticles, the assistance of AA was claimed in ref. [57]. Besides acting as reducing agent for Au overgrowth, we think AA also plays important role for sulfide shell growth in current work. AA is proposed to combine with metallic ions (Bi^{3+}, Zn^{2+}, Cu^{x+}, and Cd^{2+}) as complex and then cooperate with CTAB for carrying the metallic ions to the Au surface towards the growth of sulfide shells. Hence, different components including Bi_2S_3, CdS, ZnS, and Cu_xS nanoshells were deposited on the surface of dumbbell-like Au NRs despite of how large the lattice mismatch exists (2%–3% for Au–Bi_2S_3 and 30%–40% for Au–CdS).[56,64]

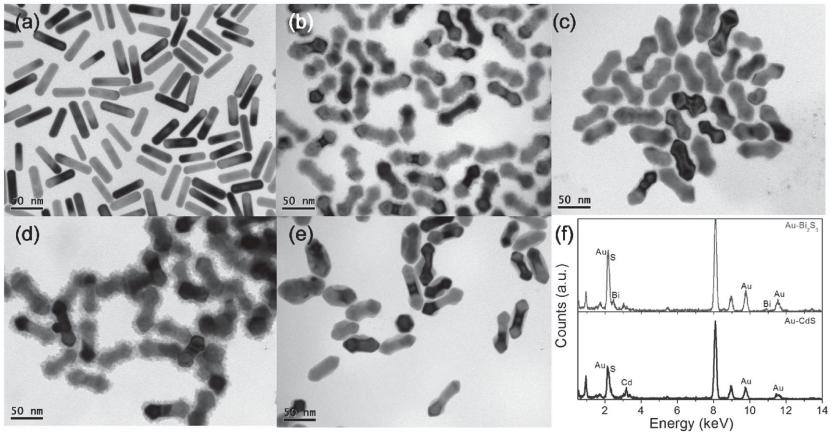

Figure 2. TEM images of initial Au NRs a), dumbbell-like Au–CdS b), Au–Bi_2S_3 c), Au–ZnS d), and Au–Cu_xS e) core–shell NRs. f) EDS spectra of dumbbell-like Au–Bi_2S_3 and Au–CdS core–shell NRs on copper grid.

The morphology and structure characterization of the dumbbell-like gold–metal sulfide core–shell NRs were performed by transmission electron microscopy (TEM). **Figure 2**a shows the initial Au NRs which have an average length/diameter of 15 ± 3 nm/55 ± 5 nm. The TEM images of dumbbell-like Au–CdS, Au–Bi_2S_3, Au–ZnS, and Au–Cu_xS NRs are shown in Figure 2b–e, respectively. All the hetero-nanostructures have uniform dumbbell-like Au cores, and the average length of dumbbell-like Au NRs is 62 ± 5 nm. The average diameters at the two ends and at the middle of the NRs are 21 ± 2 nm and 17 ± 2 nm, respectively. Both the length and diameter are increased compared with the initial Au NRs, which means the reshaping of Au NRs is due to the overgrowth of Au instead of the chemical etching. The metal sulfide shells have an average thickness of 6 ± 2 nm and it could be adjusted by controlling the amount of metal ions and the reaction time. It is easy to find that different metal sulfide had different morphology on the surface of Au NRs. For Au–CdS and Au–ZnS NRs, the nanoshells have a loose structure and they entirely encase the Au NRs. But for Au–Cu_xS and Au–Bi_2S_3 NRs, the shells exhibit a dense structure and smooth surface, while the Cu_xS layers mainly concentrate on the middle of the Au NRs. The energy dispersive X-ray spectroscopy (EDS) (Figure 2f and Figure S4, Supporting Information) and X-ray Diffraction (XRD) (Figure S5, Supporting Information) characterizations were performed to validate metallic sulfide shells. As for the EDS spectra of Au–CdS and Au–Bi_2S_3 NRs in Figure 2f, the patterns of Au, Bi, S and Au, Cd, S are clearly observed, accompanying with the other peaks generated by the copper grid.

Figure 3 displays the morphology, detailed crystallographic structures, composites, and crystalline structure of the dumbbell-like Au–Bi_2S_3–CdS hetero-nanostructure. Figure 3a shows

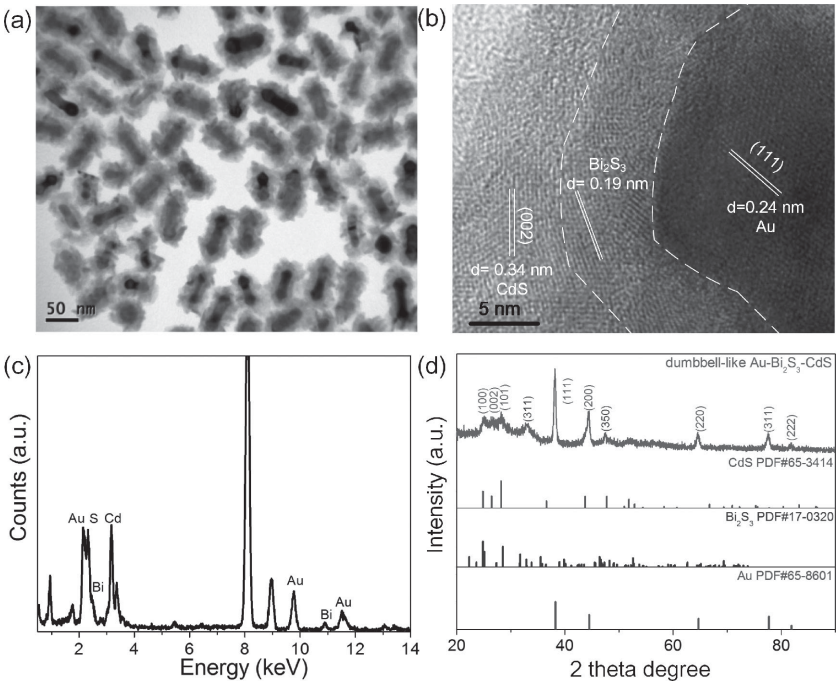

Figure 3. TEM image a), HRTEM image b), EDS spectrum c), and XRD pattern d) of dumbbell-like Au–Bi_2S_3–CdS core–shell nanostructure. The *d*-spacing value of 0.19 nm in b) could be indexed to several planes of Bi_2S_3 (including (002), (440), (431), (501), (151), (350), and (530)). The standard patterns of cubic-phase Au (PDF#65–8601), orthorhombic-phase Bi_2S_3 (PDF#17–0320), and hexagonal-phase CdS (PDF#65–3414) are displayed in d).

that the Au cores still keep uniform dumbbell-like shape and the thickness of shells increases to 15 ± 2 nm after coating CdS onto the Au–Bi_2S_3 NRs. Meanwhile, starting from the dense and smooth surface of Bi_2S_3, the shells change to loose, rough, and spinous. A high resolution TEM (HRTEM) image in Figure 3b presents the obvious double-shell structure. The lattice plane spacing of 0.24 nm in the core region agrees well with the (111) lattice planes of the fcc gold crystal.[48] The lattice plane distance of 0.34 nm in the outer shell can be ascribed to the (002) planes of CdS.[65] EDS analysis in Figure 3c verifies the composition of Au, Bi, Cd, and S in the hetero-nanostructures. The XRD pattern is shown in Figure 3d, the phases of Au, Bi_2S_3, and CdS are all observed.

2.2. Extinction Properties and Local Field Enhancement

The variation of extinction spectra dependent on the reshaping of Au NRs and coating of Bi_2S_3 and CdS are shown in **Figure 4** and the other sulfides are shown Figure S6, Supporting Information. All the samples were tested at equal amount under similar condition. The initial Au NRs exhibit two extinction bands at 514 and 780 nm, corresponding to the T-SPR and L-SPR, respectively. After the Bi_2S_3 layers were coated, the L-SPR wavelength red-shifted to 810 nm with the slight T-SPR red-shifting to 519 nm because of the increase of refractive index of the surrounding medium caused by Bi_2S_3.[48] The intensity ratio of L-SPR to T-SPR ($R = I_{\text{L-SPR}}/I_{\text{T-SPR}}$) changed little (from 3.4 to 2.5). As for the dumbbell-like Au–Bi_2S_3 NRs, the T-SPR is red-shifted to 546 nm and the L-SPR is red-shifted to 860 nm. Both of the intensities of T-SPR and L-SPR were increased and the R was decreased to 1.2. That implies the SPRs for the dumbbell-like Au–Bi_2S_3 core–shell NRs are greatly enhanced, especially for the T-SPR band, which is about 3 times than that of the initial Au NRs. The increase of T-SPR and L-SPR is mainly related to the reshaping and size enlarging of dumbbell-like Au NRs. The greatly enhanced SPRs and field distributions are displayed by the finite-difference time-domain (FDTD) simulations in Figure 4b,c. Compared with the normal Au–Bi_2S_3 NRs (the TEM images of normal Au–sulfide NRs are shown in Figure S7, Supporting Information), the local fields of L-SPR and T-SPR for the dumbbell-like Au–Bi_2S_3 NRs are all enhanced, especially for the outermost surface outside the sulfide shell, which may contribute more for the extinction intensity. It is interesting that the dumbbell-like Au–Bi_2S_3 NRs provide more hot spots of field enhancement, due to the complex shape with many sharp edges. Moreover, the multi-polar plasmon modes could be excited and overlap with the T-SPR mode, enhancing the extinction band in visible region. After coating CdS shell onto the dumbbell-like Au–Bi_2S_3 core–shell NRs, the L-SPR and T-SPR wavelengths are red-shifted to 1000 and 550 nm, respectively, which are caused by the larger dielectric constant of CdS shells as compared to Bi_2S_3 shells alone. At the same time, the intensities of L-SPR and T-SPR are further increased with R = 1.12. The dumbbell-like Au–sulfide core–shell NRs possess the advantages of the strongly enhanced T-SPRs in visible as well as the tunable L-SPRs, which indicates the materials as an ideal candidate for the high-performance optoelectronic devices.

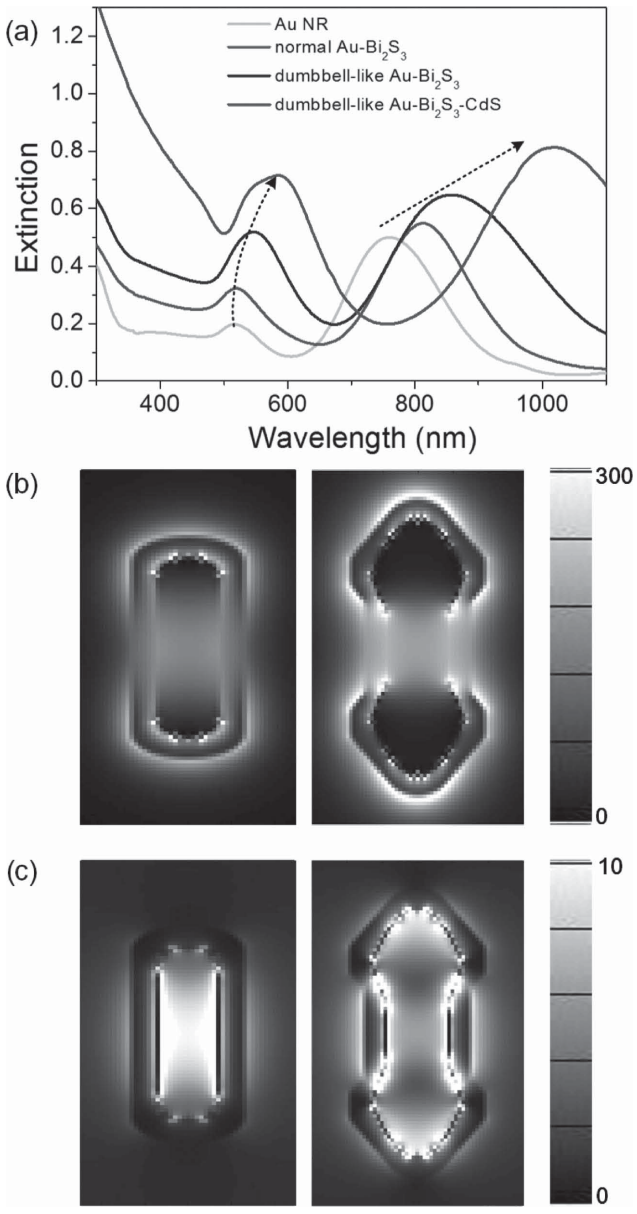

Figure 4. a) Experimental extinction spectra of dumbbell-like Au–Bi_2S_3–CdS, dumbbell-like Au–Bi_2S_3, normal Au–Bi_2S_3, and initial Au NRs. Local field distribution calculated by FDTD for dumbbell-like and normal Au–Bi_2S_3 at their L-SPR b) and T-SPR c) peaks.

2.3. Photocatalytic Activity Measurement and Mechanism Discussion

We compared the photocatalytic activity of pure Bi_2S_3 nanoparticles, normal and dumbbell-like Au–Bi_2S_3 NRs through evaluating the photodegradation of RhB. The RhB concentrations were monitored by measuring the absorption intensity of the characteristic peak at 552 nm and all the measurement were conducted under the similar conditions. As shown in **Figure 5**a, 30% and 38.8% of the dyes were reduced by pure Bi_2S_3 and normal Au–Bi_2S_3 with the irradiation for 60 min. However, for the dumbbell-like Au–Bi_2S_3, about 62% of the dyes were reduced under the same conditions, which almost has about

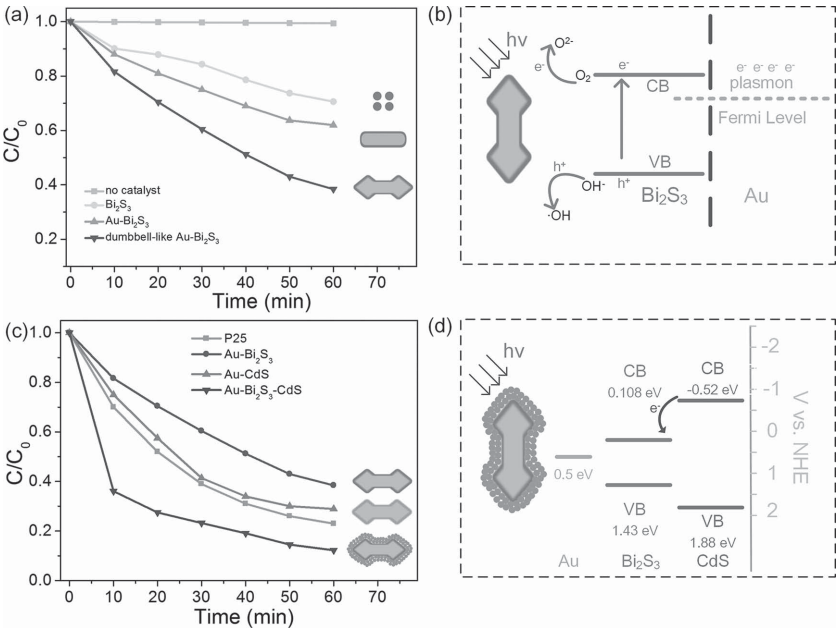

Figure 5. a) Photodegradation of RhB versus time for pure Bi_2S_3, normal and dumbbell-like Au–Bi_2S_3. b) Possible mechanism of photodegradation process of dumbbell-like Au–Bi_2S_3. c) Photodegradation of P25, dumbbell-like Au–Bi_2S_3, Au–CdS, and Au–Bi_2S_3–CdS hetero-nanostructures. d) Schematic illustration of the charge separation at the interface of dumbbell-like Au–Bi_2S_3–CdS hetero-nanostructure.

1 times enhancement as compared to pure Bi_2S_3 and about 60% to normal Au–Bi_2S_3.

Bi_2S_3 is a narrow bandgap (≈1.3 eV) semiconductor with high absorption coefficient. Here, although the Bi_2S_3 nanoparticles have the larger surface-to-volume ratio, thus the larger active surface, two Au–Bi_2S_3 hybrids show higher photocatalytic activity. The plasmon–extion interaction plays an important role. Previous literatures[66–69] discussed many possible mechanisms to elucidate the enhancement of photocatalytic activity for core–shell metal–semiconductor hetero-structures, including (i) the large local field and plasmon scattering induced absorption enhancements for semiconductor, and simultaneously, the recombination suppression for near surface photo-excited electron–hole pairs due to the short diffusion length; (ii) interfacial charge transfer from semiconductor to metal for effective charge separation; (iii) light harvesting by metal and interfacial charge transfer process, like hot electron injection from metal to semiconductor; (iv) light harvesting by metal and interfacial resonant energy transfer for electron–hole pair excitation in semiconductor. In our research, the photocatalytic activity of dumbbell-like Au–Bi_2S_3 is much better than that of normal Au–Bi_2S_3. However, the active surface for dye photodegradation is relatively small for the dumbbell-like shape because the diameter and length are increased and the surface-to-volume ratio is decreased. The pathways of (i), (iii), and (iv) play a possible role, owing to that the dumbbell-like Au–Bi_2S_3 NRs have the stronger visible T-SPR extinction and also the stronger local electric field as compared to the normal Au–Bi_2S_3 NRs.

As shown in Figure 5c, the dumbbell-like Au–Bi_2S_3–CdS core–shell NRs show the highest photocatalytic activity among the tested samples, the degradation of RhB is 64.2% at the first 10 min and 88.6% at 60 min. However, it is 19% and 62% for the dumbbell-like Au–Bi_2S_3, 25% and 71% for the dumbbell-like Au–CdS, and 30% and 77% for P25. It is easy to confirm that the photocatalytic activity of Au–Bi_2S_3–CdS is 2.5 times (1.2 times) that of Au–CdS, about 3 times (1.4 times) that of Au–Bi_2S_3, and 2.1 times (1.1 times) that of P25 at the first 10 min (60 min).

The inner charge transferring processes in photodegradation are further discussed and shown in Figure 5d to understand the mechanism of this enhanced photocatalytic activity. It is known that the bandgaps of CdS and Bi_2S_3 are 2.4 and 1.32 eV, respectively. Since electrons and holes gain energy by moving down and up, respectively,[70] the photo-excited electrons can transfer from the conduction band (CB) of CdS to the CB of Bi_2S_3. The electron transfer is occurred in the timescale of ≈10 fs.[65] Due to the relative slow migration rates for holes (10 times slower than that of electron) in valence band (VB), the photo-generated electrons and holes are spatially separated rapidly, reducing the recombination probability significantly and increasing electron lifetimes, which lead to greatly improved photocatalytic activity of dumbbell-like Au–Bi_2S_3–CdS. The investigation of ultrafast dynamic process could further reveal the picture of electron transfer and underlying mechanism. In addition, due to the double nanoshells of CdS and Bi_2S_3 as well as the intense T-SPR, visible light could be harvested more effectively (Figure S8, Supporting Information). Furthermore, the loose, rough, and spinous CdS layers shown in Figure 3a and Figure S9, Supporting Information, could provide a bigger superficial area which is very useful for the adsorbing and degradation of dye molecules.

3. Conclusion

An approach for synthesizing uniform dumbbell-like gold–sulfide core–shell nanostructures is reported in our present work. The transformation from Au NRs to dumbbell-like Au NRs and coating of metal sulfide shells (including Bi_2S_3, CdS, Cu_xS, and ZnS) were achieved in a one-pot reaction. The dumbbell-like gold NRs exhibited highly transverse plasmon resonance, strong visible light absorption, and large local electric field. Due to these excellent characters, the dumbbell-like Au–Bi_2S_3 core–shell NRs have shown better visible light photocatalytic activity as compared to pure Bi_2S_3 and normal Au–Bi_2S_3 core–shell NRs. Furthermore, the dumbbell-like Au–Bi_2S_3–CdS nanostructures with better visible light photocatalytic activity were also investigated. The optimum band configuration leads to fast electron–hole separation rate and long electron lifetimes and then produces an evident promotion to photocatalysis. We believe this synthesis approach, the dumbbell-like hetero-nanostructures as well as the underlying mechanism demonstrated

here will be useful in the photocatalytic, photoelectrochemical, and photovoltaic applications.

4. Experiment Section

Chemicals: Chloroauric acid ($HAuCl_4 \cdot 4H_2O$, 99.99%),silver nitrate ($AgNO_3$, 99.8%), glycine acid (99.5%), L-ascorbic acid (99.7%), cadmium acetate (99.5%), zinc acetate (99.5%), cupric acetate (99.5%), bismuth acetate (99.5%), thioacetamide (99%), sodium hydride (NaOH, 96%),hydrochloric acid (36%–38%), and sodium borohydride ($NaBH_4$, 96%) were purchased from Sinopharm Chemical Reagent Co. Ltd. (Shanghai, China). Hexadecyltrimethylammonium bromide (CTAB, 99.0%) was purchased from Amresco, Inc. (America). All chemicals were used as received and without further purification. All aqueous solutions were freshly prepared by using double distilled water.

Synthesis of Dumbbell-Like Gold–Metal Sulfide Core–Shell Nanorods: The CTAB-stabilized Au NRs were prepared by a seed-mediated growth method.[71] To synthesize dumbbell-like gold–metal sulfide NRs, 1 mL 0.1 M L-ascorbic acid and hexamethylenetetramine were added into 5 mL uncentrifuged Au NRs solution and 40 μL 0.1 M thioacetamide was added subsequently. The mixture solution turned to deep purple color quickly. Then 10 μL of 0.1 M metal acetate (cupric acetate, zinc acetate, bismuth acetate, or cadmium acetate) was added. The mixture solution was kept at 80 °C for 8 h in vacuum oven. The final product was centrifuged, washed, and dispersed in water for further use.

Coating Dumbbell-Like Au–Bi_2S_3Core–Shell NRs with CdS Layer: In a typical procedure, 1 mL 0.2 M glycine solution was added in dumbbell-like Au–Bi_2S_3 aqueous solution and 50 μL 0.2 M NaOH aqueous solution was injected into the mixture solution to manipulating the pH value at 7.5. Then, 120 μL 10×10^{-3} M thioacetamide and 100 μL 10×10^{-3} M cadmium acetate were added in the reaction solution, the mixture was kept at 95 °C under stirring for 4 h. The final products were centrifuged, washed, and dispersed in water for further use.

Synthesis of Normal Au–Bi_2S_3,pure Bi_2S_3, and CdS for Photocatalysis: The normal Au–Bi_2S_3 was synthesized in the similar way with dumbbell-like Au–sulfide core shell NRs except the CTAB stabilized-Au NRs should be centrifuged. Pure Bi_2S_3 and CdS also were synthesized in the absence of Au NRs. All the concentration and volume of the chemicals are the same as we mentioned before.

Photocatalytic Activity Measurement: The photocatalytic performances were measured by the photodegradation of RhB under a 300 W xenon lamp irradiation at room temperature. The 10 mg of photocatalysts were added in 30 mL 10^{-5} M aqueous solution of RhB. The mixture solution was kept continuously stirring during the irradiation and samples were taken every 10 min for further test. After removing the photocatalyst from the mixture solution by centrifugation, the concentration of the RhB was calculated by measuring the extinction density of RhB at 552 nm.

FDTD Simulations: The simulations were carried out by using FDTD method with the software FDTD Solutions 8.6. The refractive indices of Bi_2S_3 and water are 2.4 and 1.33, respectively, and that of gold is taken from ref. [72]. Perfectly matched shape and layers were used in our simulations. The Au NRs are a cylinder with round ends. The radius of the cylinder is 7 nm and radii of the ends are 5 nm and the total length of the gold rod is 50 nm. The dumbbell-like Au NRs are a cylinder with parabola cone ends. The radius of the cylinder is 7 nm, radii of the cone bottoms are 4.5 nm, height of the cones are 16 nm, and the total length of the NRs is 72 nm. All the Bi_2S_3 shell thickness is 6 nm.

Sample Characterization: The TEM and HRTEM images were obtained with a JEOL 2010 HT and a JEOL 2010 FET transmission electron microscope operated at 200 kV. EDS analysis was performed on an EDS incorporated in the HRTEM. Scanning electron microscopy (SEM) observations were performed with a FEG SEM Sirion 200 operated at an accelerating voltage of 25.0 kV. X-ray diffraction spectra (XRD) patterns were obtained on a Bruker D8 advance X-ray diffractometer with Cu–Kα irradiation ($\lambda = 0.15418$ nm). The absorption spectra were tested by UV–vis-NIR spectrophotometry (Cary 5000,Varian).

Supporting Information

Supporting Information is available from the Wiley Online Library or from the author.

Acknowledgements

L.M. and S.L. contributed equally to this work. The authors thank Yaoyao Ren and Jinwen Yang for the TEM measurement. The authors also thank Dingze Lu for the XRD measurement. This work was supported in part by the National Program on Key Science Research of China (Grant No. 2011CB922201), and the NSFC (Grant Nos. 11174229 and 11374236).

Received: September 29, 2014
Revised: November 21, 2014
Published online: December 22, 2014

[1] B. O'regan, M. Grätzel, *Nature* **1991**, *353*, 737.
[2] K. Hashimoto, H. Irie, A. Fujishima, *Jpn. J. Appl. Phys.* **2005**, *44*, 8269.
[3] S. Han, L. Hu, N. Gao, A. Al-Ghamadi, X. Fang, *Adv. Funct. Mater.* **2014**, *24*, 3725.
[4] A. Mclaren, T. Valdes-Solis, G. Li, S. C. Tsang, *J. Am. Chem. Soc.* **2009**, *131*, 12540.
[5] J. L. Yang, S. J. An, W. I. Park, G.-C. Yi, W. Choi, *Adv. Mater.* **2004**, *16*, 1661.
[6] F. Lu, W. Cai, Y. Zhang, *Adv. Funct. Mater.* **2008**, *18*, 1047.
[7] M. Ni, M. H. K. Leung, D. C. Y. Leung, K. Sumathy, *Renewable Sustain. Energy Rev.* **2007**, *11*, 401.
[8] A. B. F. Martinson, J. W. Elam, J. T. Hupp, M. J. Pellin, *Nano Lett.* **2007**, *7*, 2183.
[9] K. Woan, G. Pyrgiotakis, W. Sigmund, *Adv. Mater.* **2009**, *21*, 2233.
[10] X. Liu, L. Pan, T. Lv, G. Zhu, Z. Sun, C. Sun, *Chem. Commum.* **2011**, *47*, 11984.
[11] Y. Wang, R. Shi, J. Lin, Y. Zhu, *Energy Environ. Sci.* **2011**, *4*, 2922.
[12] J. Zhang, Y. Tang, K. Lee, M. Ouyang, *Nature* **2010**, *466*, 91.
[13] S. H. Woo, W. C. Na, I. D. Kim, H. J. Lee, *Nanotechnology* **2012**, *23*, 245501.
[14] C. T. Yuan, G. Y. Wang, K. Y. Huang, T. Y. Chen, P. Yu, J. Tang, A. Sitt, U. Banin, O. Millo, *ACS Nano* **2011**, *6*, 176.
[15] L. T. Su, S. K. Karuturi, J. Luo, L. Liu, X. Liu, J. Guo, T. C. Sum, R. Deng, H. J. Fan, X. Liu, A. L. Y. ToK, *Adv. Mater.* **2013**, *25*, 1603.
[16] K. K. Haldar, N. Pradhan, A. Patra, *Small* **2013**, *9*, 3424.
[17] X. Xu, L. Hu, N. Gao, S. Liu, S. Wageh, A. A. Al-Ghamdi, A. Alshahrie, X. Fang, *Adv. Funct. Mater.* **2014**, DOI: 10.1002/adfm.201403065.
[18] S. K. Cushing, J. Li, F. Meng, T. R. Senty, S. Suri, M. Zhi, M. Li, A. D. Bristow, N. Wu, *J. Am. Chem. Soc.* **2012**, *134*, 15033.
[19] Z. Liu, W. Hou, P. Pavaskar, M. Aykol, S. B. Cronin, *Nano Lett.* **2011**, *11*, 1111.
[20] P. Li, Z. Wei, T. Wu, Q. Peng, Y. Li, *J. Am. Chem. Soc.* **2011**, *133*, 5660.
[21] M. W. Knight, Y. Wang, A. S. Urban, A. Sobhani, B. Y. Zheng, P. Nordlander, N. J. Halas, *Nano Lett.* **2013**, *13*, 1687.
[22] S. C. Warren, E. Thimsen, *Energy Environ. Sci.* **2012**, *5*, 5133.
[23] C. Clavero, *Nat. Photonics* **2014**, *8*, 95.
[24] W. Wang, S. Wu, K. Reinhardt, Y. Lu, S. Chen, *Nano Lett.* **2010**, *10*, 2012.
[25] H. Chen, M. G. Blaber, D. S. Standridge, E. J. DeMarco, J. T. Hupp, M. A. Ratner, G. C. Schatz, *J. Phys. Chem. C* **2012**, *116*, 10215.
[26] H. A. Atwater, A. Polman, *Nat. Mater.* **2010**, *9*, 205.
[27] S. W. Hsu, K. On, A. R. Tao, *J. Am. Chem. Soc.* **2011**, *133*, 19072.
[28] C. An, S. Peng, Y. Sun, *Adv. Mater.* **2010**, *22*, 2570.

[29] Y. Tian, T. Tatsuma, *J. Am. Chem. Soc.* **2005**, *127*, 7632.
[30] T. Hirakawa, P. V. Kamat, *Langmuir* **2004**, *20*, 5645.
[31] P. Wang, T. F. Xie, H. Y. Li, L. Peng, Y. Zhang, T. S. Wu, S. Pang, Y. F. Zhao, D. J. Wang, *Chem. Eur. J.* **2009**, *15*, 4366.
[32] R. G. Chaudhuri, S. Paria, *Chem. Rev.* **2011**, *112*, 2373.
[33] G. A. Sotiriou, A. M. Hirt, P. Y. Lozach, A. Tekeki, F. Krumeich, S. E. Pratsinis, *Chem. Mater.* **2011**, *23*, 1985.
[34] E. C. Cho, L. Au, Q. Zhang, Y. Xia, *Small* **2010**, *6*, 517.
[35] A. K. Samal, L. Polavarapu, S. Rodal-Cedeira, L. M. Liz-Marzán, J. PérezJuste, I. Pastoriza-Santos, *Langmuir* **2013**, *29*, 15076.
[36] M. L. Personick, M. R. Langille, J. Zhang, C. A. Mirkin, *Nano Lett.* **2011**, *11*, 3394.
[37] Y. Wang, Y. Zheng, C. Z. Huang, Y. Xia, *J. Am. Chem. Soc.* **2013**, *135*, 1941.
[38] M. Chen, B. Wu, J. Yang, N. Zheng, *Adv. Mater.* **2012**, *24*, 862.
[39] L. Vigderman, B. P. Khanal, E. R. Zubarev, *Adv. Mater.* **2012**, *24*, 4811.
[40] C. Wang, Z. Ma, T. Wang, Z. Su, *Adv. Funct. Mater.* **2006**, *16*, 1673.
[41] C. Fang, H. Jia, S. Chang, Q. Ruan, P. Wang, T. Chen, J. Wang, *Energy Environ. Sci.* **2014**, *7*, 3431.
[42] C. H. Kuo, T. E. Hua, M. H. Huang, *J. Am. Chem. Soc.* **2009**, *131*, 17871.
[43] A. Gole, J. W. Stone, W. R. Gemmill, H. C. Loye, C. J. Murphy, *Langmuir* **2008**, *24*, 6232.
[44] B. Li, T. Gu, T. Ming, J. Wang, P. Wang, J. Wang, J. C. Wang, *ACS Nano* **2014**, *8*, 8152.
[45] M. Li, X. F. Yu, S. Liang, X. N. Peng, Z. J. Yang, Y. L. Wang, Q. Q. Wang, *Adv. Funct. Mater.* **2011**, *21*, 1788.
[46] H. Wang, Z. Sun, Q. Lu, F. Zeng, D. Su, *Small* **2012**, *8*, 1167.
[47] F. Nan, S. Liang, J. H. Wang, X. L. Liu, D. J. Yang, X. F. Yu, L. Zhou, Z. H. Hao, Q. Q. Wang, *Adv. Opt. Mater.* **2014**, *2*, 679.
[48] Z. Sun, Z. Yang, J. Zhou, M. H. Yeung, W. Ni, H. Wu, J. Wang, *Angew. Chem. Int. Ed.* **2009**, *48*, 2881.
[49] M. Grzelczak, A. Sánchez-Iglesias, B. Rodríguez-González, R. Alvarez-Puebla, J. Pérez-Juste, L. M. Liz-Marzán, *Adv. Funct. Mater.* **2008**, *18*, 3780.
[50] C. J. Huang, P. H. Chiu, Y. H. Wang, C. F. Yang, *J. Colloid Interface Sci.* **2006**, *303*, 430.
[51] X. Kou, S. Zhang, Z. Yang, C. K. Tsung, G. D. Stucky, L. Sun, J. Wang, C. Yan, *J. Am. Chem. Soc.* **2007**, *129*, 6402.
[52] F. Ratto, P. Matteini, F. Rossi, R. Pini, *J. Nanopart. Res.* **2010**, *12*, 2029.
[53] B. Rodríguez-González, F. Attouchi, M. F. Cardinal, V. Myroshnychenko, O. Stéphan, F. J. García de Abajo, L. M. Liz-Marzán, M. Kociak, *Langmuir* **2012**, *28*, 9063.
[54] M. Grzelczak, A. Sánchez-Iglesias, H. H. Mezerji, S. Bals, J. Pérez-Juste, L. M. Liz-Marzán, *Nano Lett.* **2012**, *12*, 4380.
[55] C. B. Roxlo, B. Abeles, T. Tiedje, *Phys. Rev. Lett.* **1984**, *52*, 1994.
[56] J. Zhang, Y. Tang, K. Lee, M. Ouyang, *Science* **2010**, *327*, 1634.
[57] Y. Yang, S. Han, G. Zhou, L. Zhang, X. Li, C. Zou, S. Huang, *Nanoscale*, **2013**, *5*, 11808.
[58] B. N. Khlebtsov, V. A. Khanadeev, J. Ye, G. B. Sukhorukov, N. G. Khlebtsov, *Langmuir* **2014**, *30*, 1696.
[59] L. Scarabelli, M. Grzelczak, L. M. Liz-Marzán, *Chem. Mater.* **2013**, *25*, 4232.
[60] C. C. Huang, Z. Yang, H. T. Chang, *Langmuir* **2004**, *20*, 6089.
[61] M. Li, Z. S. Zhang, X. Zhang, K. Y. Li, X. F. Yu, *Opt. Express* **2008**, *16*, 14288.
[62] J. H. Song, F. Kim, D. Kim, P. Yang, *Chem. Eur. J.* **2005**, *11*, 910.
[63] D. A. Zweifel, A. Wei, *Chem. Mater.* **2005**, *17*, 4256.
[64] G. Manna, R. Bose, N. Pradhan, *Angew. Chem. Int. Ed.* **2014**, *126*, 6861.
[65] Z. Fang, Y. Liu, Y. Fan, Y. Ni, X. Wei, K. Tang, J. Shen, Y. Chen, *J. Phys. Chem. C* **2011**, *115*, 13968.
[66] V. Subramanian, E. E. Wolf, P. V. Kamat, *J. Am. Chem. Soc.* **2004**, *126*, 4943.
[67] W. Hou, S. B. Cronin, *Adv. Funct. Mater.* **2013**, *23*, 1612.
[68] S. K. Cushing, J. Li, F. Meng, T. R. Senty, S. Suri, M. Zhi, M. Li, A. D. Bristow, N. Wu, *J. Am. Chem. Soc.* **2012**, *134*, 15033.
[69] N. Zhou, L. Polavarapu, N. Gao, Y. Pan, P. Yuan, Q. Wang, Q. H. Xu, *Nanoscale* **2013**, *5*, 4236.
[70] R. Marschall, *Adv. Funct. Mater.* **2014**, *24*, 2421.
[71] N. R. Jana, L. Gearheart, C. J. Murphy, *J. Phys. Chem. B* **2001**, *105*, 4065.
[72] P. B. Johnson, R. W. Christy, *Phys. Rev. B* **1972**, *6*, 4370.